Thermophysics and Aeromechanics, *2021*, *Vol. 28*, *No. 5*

DOI: 10.1134/S0869864321050036

Flows visualization for a supersonic mixing layer behind the blunt trailing edge under non-isobaric initial conditions*

R. Yang, Yu. Zhao, and Zh. Wang

National University of Defense Technology, *Changsha*, *China*

E-mail: yangrui11@nudt.edu.cn

(*Received November 12*, *2019*; *revised March 25*, *2020*;
accepted for publication August 05, *2020*)

Nano-tracer Planar Laser Scattering (NPLS) technique and pseudo-color processing technology are employed to investigate the flow field after a thickness plate of non-isobaric initial conditions. The results show that the supersonic mixing layer behind the blunt trailing edge will deflect toward the low pressure side which is consistent with the canonical mixing layer. However, there is no laminar region for any unmatched cases and the turbulent state of the mixing layer seems to be restricted for the case of the low-speed side with a higher pressure.

Keywords: NPLS, mixing layer, pseudo-color processing.

The supersonic blunt trailing edge flows are common in high-speed flight regime, typically exiting in the afterbody flow field of a missile or a blunted airfoil. Recently, researchers have found that the growth rate of mixing layer after a finite thick plate increases more significantly than in the thin trailing edge case [1, 2], which brings a new idea to enhance the mixing of freestream and fuel [3]. Most of previous works were usually conducted on the matched pressure condition, meaning that the pressure was almost equal for both sides of mixing layer. Whereas, it is difficult to maintain the matched pressure for actual flow field, besides the mixing layer is deliberately designed to be non-isobaric for some engineering applications.

The authors of [4] claimed that the unmatched pressure was the reason for the discrepancy between the prediction model and the experimental data, but there was no further explanation. It was found in [5] that the effect of non-isobaric to the mixing layer thickness, after many successive interactions with reflected waves, could be negligible. A similar conclusion was reached by the authors of [6] with the laser Doppler velocimeter. They pointed out the asymptotic state of the mixing layer was the same regardless of the initial pressure conditions. One moderate influence was the advancement of the mixing layer transition position for unmatched conditions. However, it was found in [7] that the fluctuation of the angle of the location of shear layer structures significantly increased compared to matched cases, which would influence the eddy shedding frequency, and then extremely decrease the passive scalar

* The work was financially supported by National Natural Science Foundation of China (Grant No. 11172324).

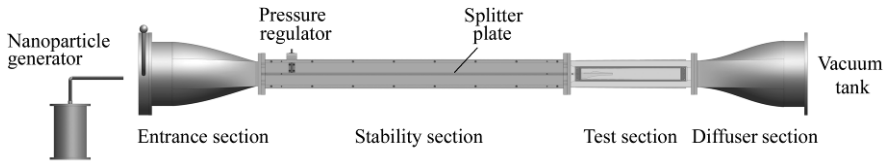

Fig. 1. Supersonic mixing layer wind tunnel.

convection speeds. The authors of [8] firstly adopted Nano-tracer Planar Laser Scattering (NPLS) technique to get the fine flow field structures of the thin mixing layer. They discovered that the vortex broke into a smaller scale earlier due to the unmatched pressure. Meanwhile, they explained that the increase of boundary layer thickness for the lower pressure side, caused by the higher pressure of downstream, essentially enhanced the turbulence level of the mixing layer. However, the interpretation is implausible for the mixing layer with a base region, as the base pressure in the recirculation region is relatively constant [9].

In this paper, the effect of three different initial pressure conditions, typically representing the matched case for $p_1/p_2 = 1.0$ and the unmatched cases (overexpanded and underexpanded flows for $p_1/p_2 = 0.5$ and 2.0, respectively), to the supersonic planar mixing layer after a finite thickness plate are investigated with NPLS technique.

Supersonic suction wind tunnel with a double nozzle for the Mach numbers 1.5 and 2.5 for upper and lower side, respectively, is used in the experimental investigation (see Fig. 1). The tunnel is composited of the entrance section, stability section, test section, and diffuser section. Its downstream is connected with a 1000 m^3 spherical vacuum tank. A splitter plate is mounted in the middle of the wind tunnel, thus dividing the flow channel into two. The nozzle contours are designed by the characteristic line method with B-spline curve. The entrance in the nozzle is under the atmosphere conditions under which the pressure and the temperature are 1 atm and 300 K, respectively. With the help of the stability section and the nozzle contour [10], the turbulence intensity at the nozzle outlet can be controlled under 0.5 %. In this way, the flow state near the trailing edge can remain laminar. The nanoparticle generator is like a fluidized bed. Numerous TiO_2 particles with the particle size of about 50 – 200 nm are shifted by high-pressure gas and seeded in the freestream. After a long distance of mixing, the particles are evenly dispersed in the flow before the test section.

The experimental model is shown in Fig. 2. The spanwise length $L = 200$ mm to ensure a planar mixing layer in the test section, and the blunt trailing edge $h = 10$ mm. The height of the test section is 50 mm. NPLS technique [11] is utilized to get the high temporal-spatial resolution flow structures of the flow field. A dual-cavity Nd:YAG laser system is employed to illuminate the flow field area. It can produce two lasers with the wavelength of 532 nm and maximum energy of 520 mJ in 6 ns (±1 ns) interval. The average thickness of the laser sheet light in the test area is about 0.5 mm, which effectively avoids the blur caused by the superposition of space. With the help of synchronization controller, CCD camera can catch the instantaneous flow field image. The images are recorded by Nikon D70s digital CCD camera which has an array of 4000×4000 pixels. According to the sizes of the experimental observation area, the spatial resolution of the image is approximately 27.5 μm/pixel.

To achieve unmatched pressure conditions, a total pressure-regulating valve is mounted in the upstream from the nozzle of the upper side as shown in Figs. 1 and 3. Because the inflows of the two sides are the same, the pressure of the upper side at the exit of nozzle is about 4.6 times that of the lower side according to the isentropic flow theory. The major components are three multi-orifices and a regulator. By revolving the stem to alter the position of the middle plate, the flow channel area can be reduced resulting in less fluid flux per unit time. In this way, the total pressure of freestream can be changed. In this work, the pressure of the lower side remains the same, the unmatched pressure conditions can be achieved by simply changing the pressure on the upper side.

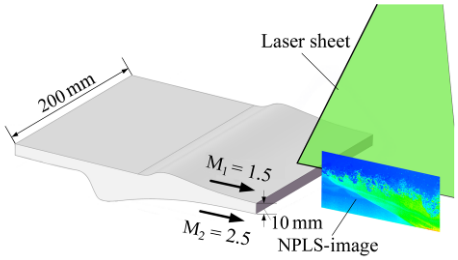

Fig. 2. Sketch of the experimental model.

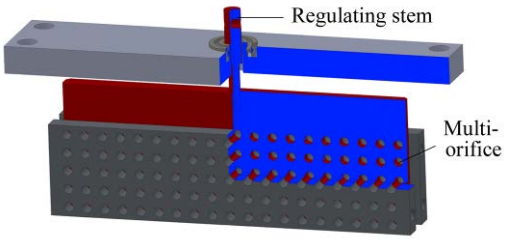

Fig. 3. The 3/4 model of total pressure-regulator.

A gray-to-color pretreatment [12] is adopted to reduce the noise of experimental images and makes the flow structures more visual. And it is important to note that the colors only give a hand to identify the structures in the flow field and represent the density in a specific figure.

The panorama for three different pressure conditions is shown in Fig. 4. Solid lines here roughly indicate the lower edge of the mixing layer. Three red lines are parallel and correspond to case 4*b*. It illustrates the pressure conditions can indeed affect the direction of development of the mixed layer, although the impact is small. The mixing layer always deflects to the lower pressure side, which is consistent with the conclusions made in [6]. Meanwhile, the deflection angle, 1.7° for case 4*a* and 2.2° for case 4*c*, seems to be related to the upper and lower pressure ratio p_1/p_2. The panorama is facilitated to recognize the development of mixing layer, but not good for the insight of flow mechanism. Therefore, the flow from 0 to 50 mm downstream of the plate base is further recorded.

Figure 5 depicts the typical near flow field of three cases. They generally have the same flow field structure. The two boundary layers separate from the plate base and undergo strong dilation, transform into separate shear layers. Then the two shear layers encounter each other and form a reattachment point, which is denoted by pentacle in figure. After impingement, the two shear layers are re-organized to form a redevelopment mixing layer. We can find that the mixing layer immediately converts into turbulence after the reattachment point and there is no laminar region that is usual for the mixing layer after a thin trailing edge [11]. One possible reason is that the separated shear layers separate high-speed inviscid flow and low-speed wake with a recirculation zone. With large velocity gradient, high compressibility and strong turbulent flow characteristics, the free-shear layers have significant effects on the dynamics of wake [13]. Another important factor is the impingement of the two, causing extreme instability in the wake. These terrifically complex flow field features of the supersonic wake have brought great challenges to the study of its stability [14].

Meanwhile, it seems that the turbulence level of the separated shear layer for the lower pressure side will be restrained by comparing Figs. 5*b* and 5*c*. Another notable feature is that

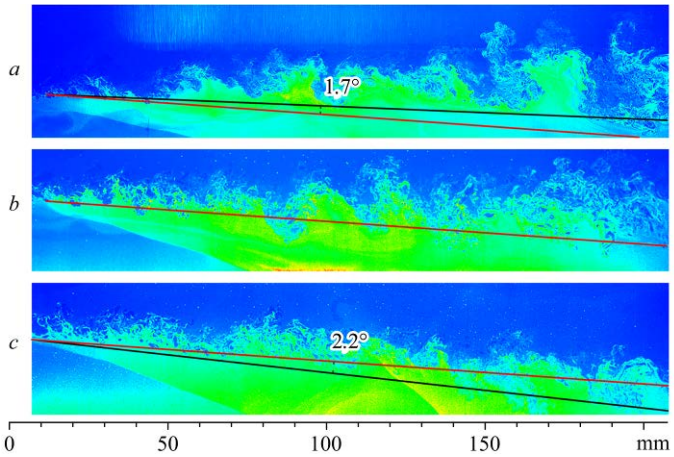

Fig. 4. The panorama of the supersonic blunt trailing edge for $p_1/p_2 = 0.5$ (*a*), 1.0 (*b*), and 2.0 (*c*).

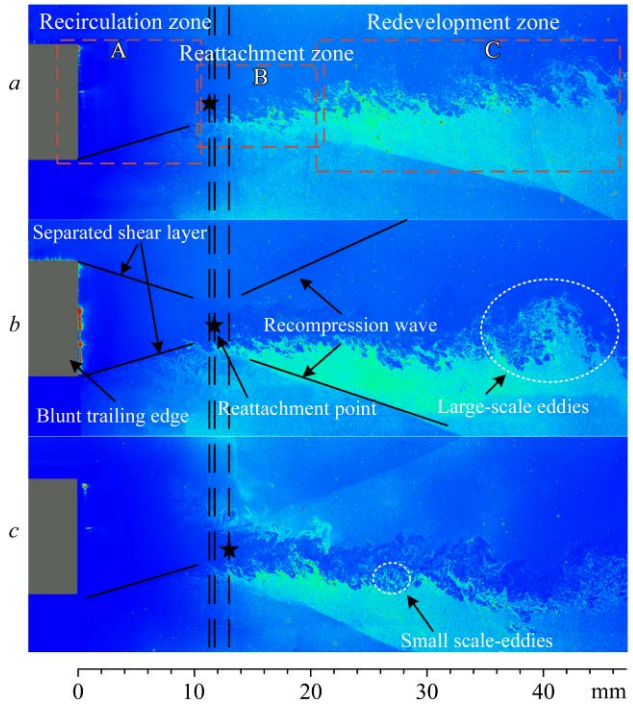

Fig. 5. The near flowfield of three conditions: $p_1 / p_2 = 0.5$ (*a*), 1 (*b*), and 2 (*c*).

there are usually small-scale eddies for the underexpansion case. Through comparing the intersection point of the lower recompression wave and the bottom margin, it comes to the same conclusion that the pressure ratio does influence the deflection angle of the mixing layer. But it seems that the overexpanded case has even greater impact from this aspect, which is different from the perspective of the panorama.

To summarize, with utilizing NPLS technique and pseudo-color processing technology, fine flow field structures after a finite thickness plate are acquired. The mixing layer tends to deflect to the lower pressure side, while the extent is different from different perspectives. A more reasonable criterion needs to be proposed further. The initial state of the mixing layer is turbulent at the very start, which is quite different from the canonical mixed layer. However, the turbulent state of the mixing layer seems to be restricted when the low-speed side has a higher pressure.

References

1. **S. Laizet and E. Lamballais,** Direct numerical simulation of a spatially evolving flow from an asymmetric wake to a mixing layer, Direct and Large-Eddy Simulation VI, 2006, P. 467–474.
2. **S. Laizet, S. Lardeau, and E. Lamballais,** Direct numerical simulation of a mixing layer downstream a thick splitter plate, Phys. Fluids, 2010, Vol. 22, No. 1, 015104.
3. **T. Reedy,** Control of supersonic axisymmetric base flows using passive splitter plates and pulsed plasma actuators, University of Illinois at Urbana-Champaign, 2014.
4. **L.W. Tufts and L.D. Smoot,** A turbulent mixing coefficient correlation for coaxial jets with and without secondary flows, J. Spacecr. Rock., 1971, Vol. 8, No. 12, P. 1183–1190.
5. **M. Samimy, G.S. Elliott, D.D. Glawe, M.F. Reeder, and S.A. Arnefte,** Compressible mixing layers with and without particles, Ohio St. Univer., 1992.
6. **S. Barre, P. Braud, O. Chambres, and J.P. Bonnet,** Influence of inlet pressure conditions on supersonic turbulent mixing layers, Experimental Thermal and Fluid Science, 1997, Vol. 14, No. 1, P. 68–74.
7. **R. Mahadevan, E. Loth, and J. Dutton,** Effect of an expansion-compression wave pair on free shear layer dynamics, in: 33rd Aerospace Sciences Meeting and Exhibit, 1995.
8. **Y. Zhao, L. Tian, S. Yi, L. He, and Z. Cheng,** Experimental study of flow structure in pressure unmatched mixing layer, J. Experim. Fluid Mech., 2007, Vol. 21, No. 2 P. 14–17.
9. **V.A. Amatucci, J.C. Dutton, D.W. Kuntz, and A.L. Addy,** Two-stream, supersonic, wake flowfield behind a thick base. I - General features, AIAA Journal, 1992, Vol. 30, No. 8, P. 2039–2046.
10. **Y. Zhao, S. Yi, L. Tian, L. He, and Z. Cheng,** Multiresolution analysis of density fluctuation in supersonic mixing layer, Science China Technological Sciences, 2010, Vol. 53, No. 2, P. 584–591.
11. **Y. Zhao, S. Yi, L. Tian, and Z. Cheng,** Supersonic flow imaging via nanoparticles, Science in China Series E: Technological Sciences, 2009, Vol. 52, No. 12, P. 3640–3648.
12. **Y. Zhao, Z. Wang, Y. Zhao, and X. Fan,** Visualization of massive separation of unstarted inlet, J. Visualization, 2014, Vol. 17, No. 4, P. 299–302.
13. **B.M. Kirchner, T.J. Tetef, J.C. Dutton, and G.S. Elliott,** Three-Dimensional Entrainment Dynamics of a Supersonic Base Flow, AIAA Scitech 2019 Forum, 2019.
14. **C.D. Kazemba, R.D. Braun, I.G. Clark, and M. Schoenenberger,** Survey of blunt-body supersonic dynamic stability, J. Spacecraft and Rockets, 2012, Vol. 54, No. 1, P. 109–127.